Supporting Information for:

Breaking the Cycle: Impact of Sterically-Tailored Tetra(pyrazolyl)lutidines on the Self-Assembly of Silver(I) Complexes

Tyler J. Morin, Andrew Merkel, Sergey V. Lindeman, and James R. Gardinier.*

Department of Chemistry, Marquette University, Milwaukee, WI 53201-1881.

Table of Contents:

Figure S-1. ORTEP diagram (ellipsoids drawn at 50% probability level) of three independent units of **pz$_4$lut**, each with different conformations of pyrazolyls.

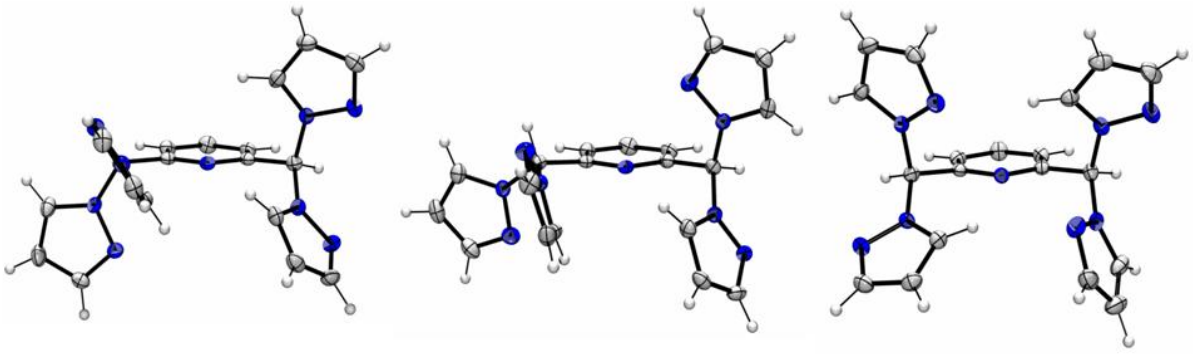

Figure S-2. ORTEP diagram (ellipsoids drawn at 50% probability level) of **pz*$_4$lut**.

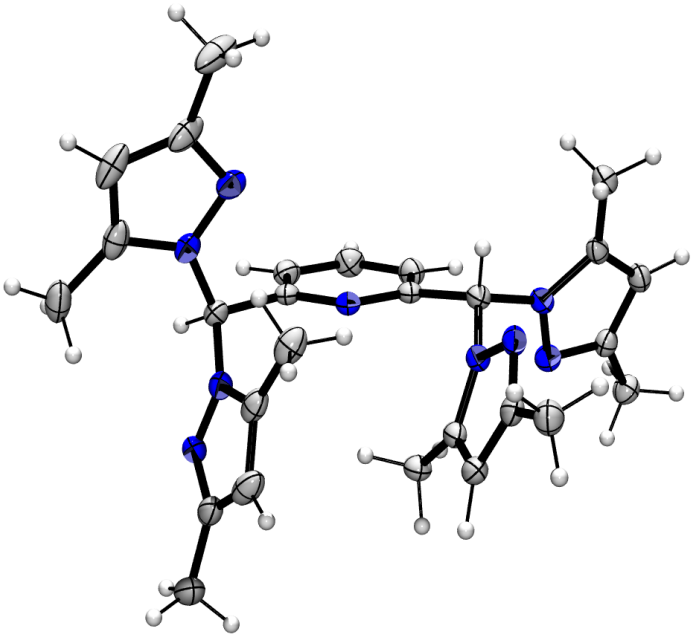

Figure S-3. Supramolecular structure of **1.**

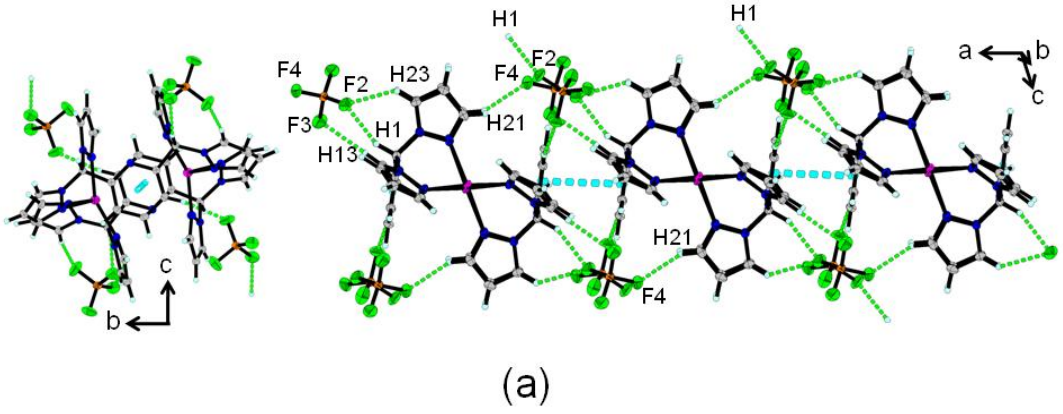

(a)

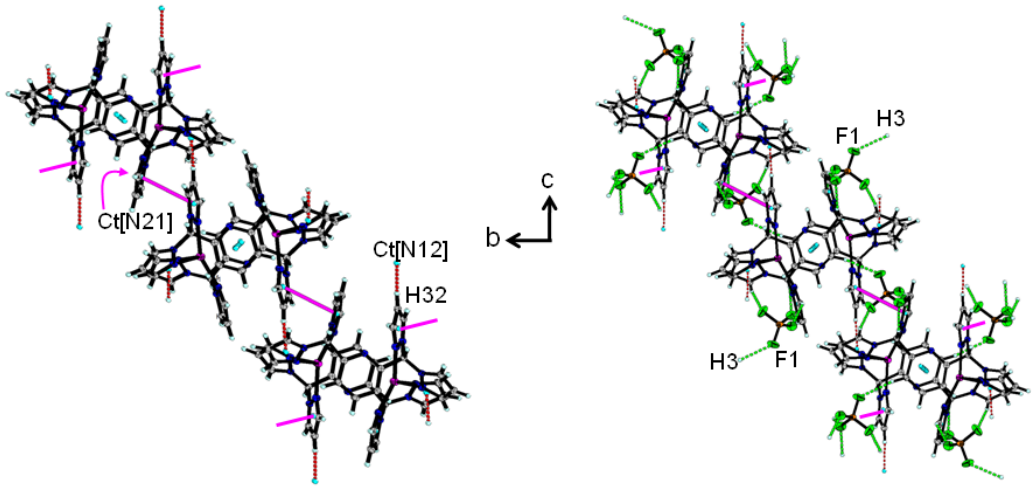

(b)

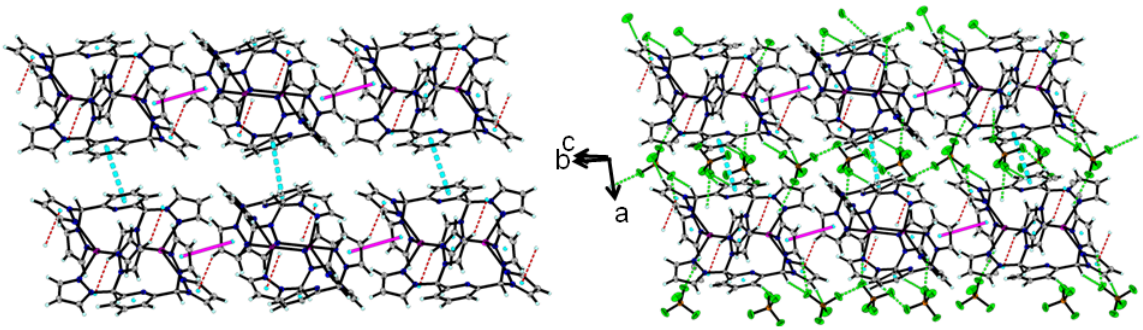

(c)

Figure S-4. Organizing features of the 3D supramolecular structure in **2**·CH_3CN**.**

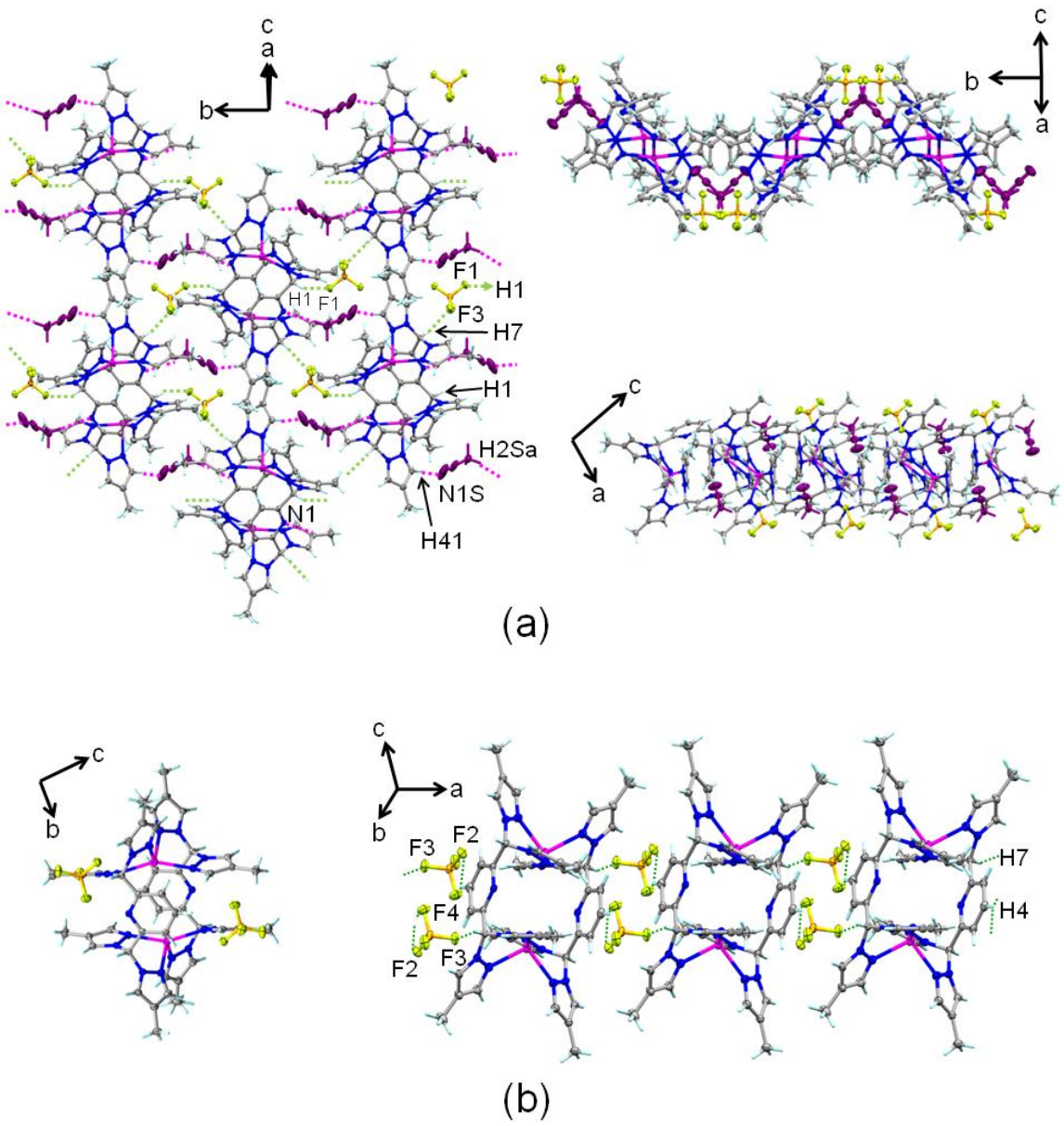

Figure S-5. Organizing features of the 3D supramolecular structure in **3**·CH_3CN**.**

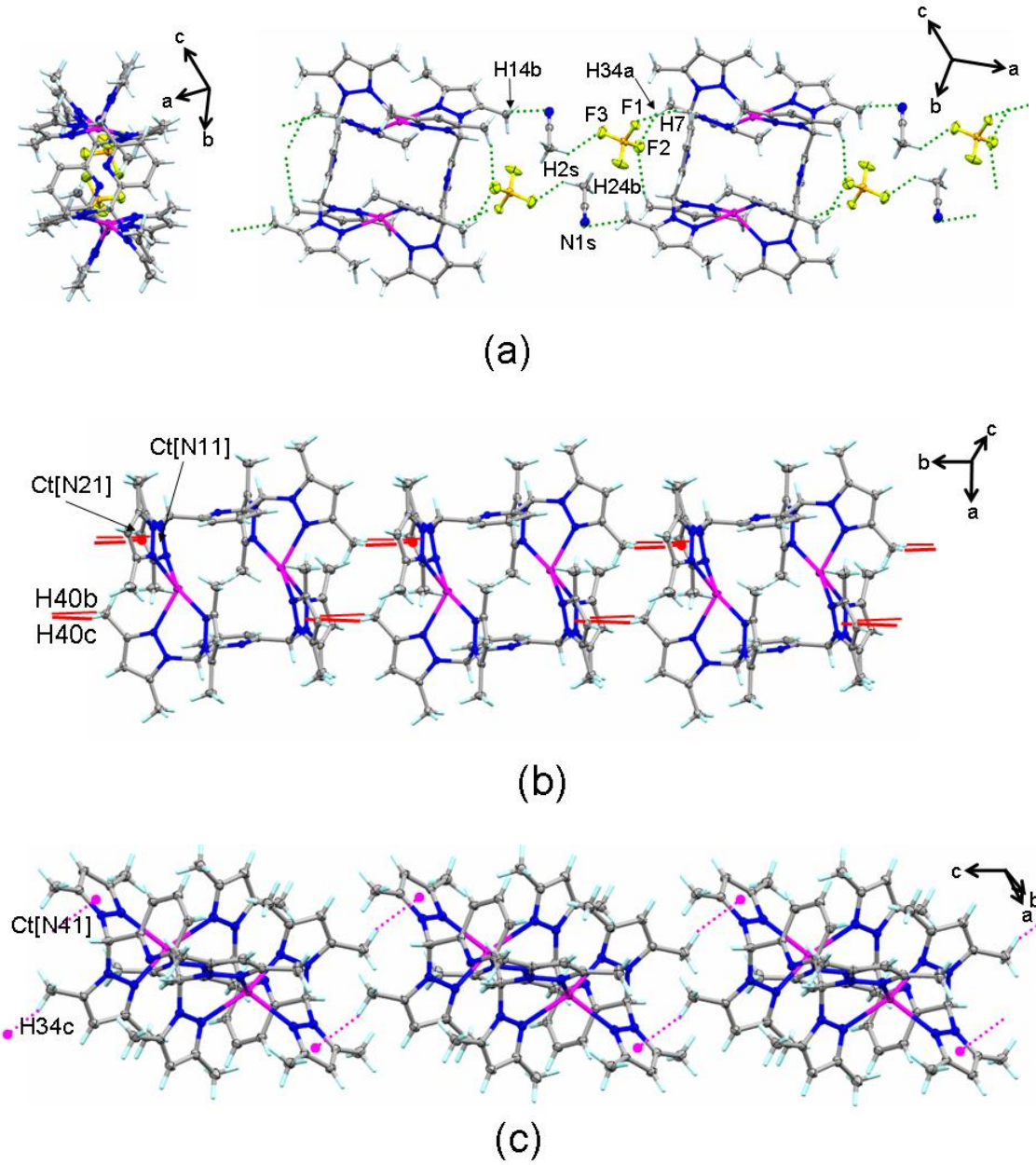

Figure S-6. View of the crystal packing diagram of **5** along the *a*-axis**.**

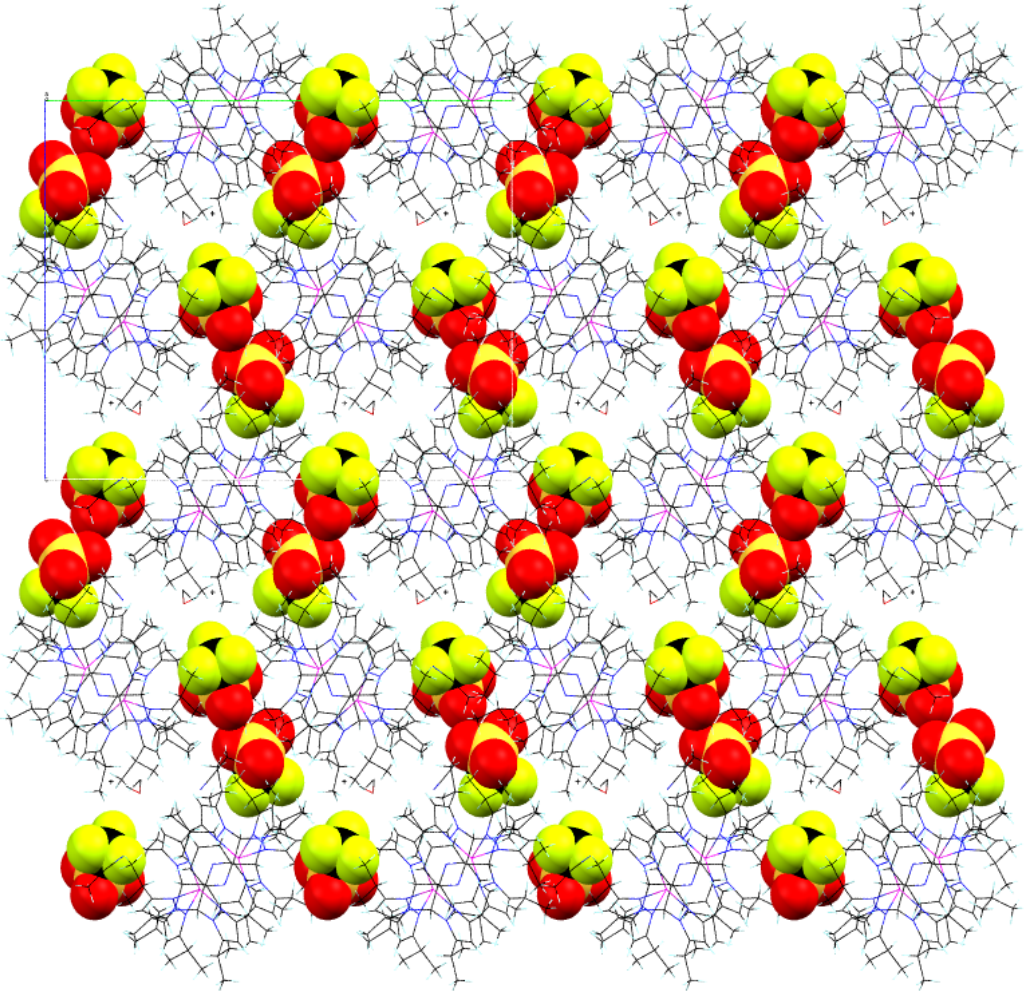

Table S-1. Summary of "Intermolecular" Noncovalent Interactions in **1**, **2**·CH_3CN, and **3**·CH_3CN.

(a) Compound **1**

π-π interactions	Ct-Ct (Å)	α(°)	β(°)	γ(°)	perp(Å)
Ct[py] ··Ct[py]	3.7338(10)	0	12.74	12.74	3.6419(7)
Ct[N21] ··Ct[N31]	3.6153(11)	17.20	15.05	31.26	-3.09, 3.49
Donor-H ··Acceptor	D-H (Å)	H ··A (Å)	D ··A (Å)	D-H ··A (°)	
C32H32 ··Ct[N11]	0.95	2.59	3.427(2)	148	
C1H1 ··F2	1.00	2.23	3.162(2)	155	
C3H3 ··F1	0.95	2.44	3.377(2)	167	
C7H7 ··F1	1.00	2.48	3.425(2)	157	
C12H12 ··F4	0.95	2.54	3.448(2)	160	
C13H13 ··F3	0.95	2.43	3.375(2)	170	
C21H21 ··F4	0.95	2.42	3.178(2)	136	
C23H23 ··F2	0.95	2.40	3.148(2)	136	
C33H33 ··F3	0.95	2.54	3.427(2)	155	
C43H43 ··F1	0.95	2.52	3.304(2)	140	

(b) Compound **2**·CH_3CN

Donor-H ··Acceptor	D-H (Å)	H ··A (Å)	D ··A (Å)	D-H ··A (°)
C1H1 ··F1	0.93(2)	2.38	3.257(2)	157
C2SH2Sa ··N1	0.99(3)	2.49	3.458(3)	166
C2SH2Sb ··F1	0.98(3)	2.52	3.285(3)	135
C4H4 ··F2	0.94(2)	2.53	3.216(2)	131
C4H4 ··F4	0.94(2)	2.54	3.423(2)	158
C7H7 ··F3	0.94(2)	2.27	3.171(2)	160
C13H13 ··F1	0.92(2)	2.50	3.269(2)	141
C23H23 ··F3	0.90(2)	2.49	3.180(2)	134
C24H24a ··F4	0.93(3)	2.54	3.352(3)	146
C41H41 ··N1S	0.89(2)	2.51	3.384(4)	166
C43H43 ··F2	0.93(2)	2.51	3.404(2)	162

(c) Compound **3**·CH_3CN

Donor-H ··Acceptor	D-H (Å)	H ··A (Å)	D ··A (Å)	D-H ··A (°)
C34H34c ··Ct[N41]	0.93(3)	2.80(2)	3.590(2)	139(2)
C40H40b ··Ct[N21]2	0.95(3)	2.98(3)	3.874(3)	156(3)
C40H40c ··Ct[N11]	0.95(3)	2.69(4)	3.486(3)	146(3)
C2SH2Sb ··F3	0.95(4)	2.50(4)	3.436(4)	166(3)
C2SH2Sc ··F3	1.04(3)	2.38(4)	3.086(4)	124(3)
C4H4 ··F4	0.95(2)	2.53(2)	3.470(3)	172(2)
C7H7 ··F1	0.93(2)	2.47(2)	3.173(3)	133(2)
C12H12 ··N1S	0.93(3)	2.60(3)	3.466(3)	155(2)
C14H14b ··N1S	1.01(4)	2.55(4)	3.371(3)	139(3)
C24H24b ··F2	0.95(3)	2.47(3)	3.395(3)	167(3)
C34H34a ··F2	0.93(3)	2.39(3)	3.260(3)	157(2)
C44H44c ··F1	0.95(3)	2.52(3)	3.279(3)	137(2)

Discussion of supramolecular structures of 1-3. The supramolecular structure of **1** is three dimensional as a result of three sets of π-π and CH-π non-covalent interactions between heterocyclic rings[S1] of cations, five very short (less than 2.47 Å, the sum of the van der Waals radii, $\Sigma^{vdw}_{H\text{-}F}$, of H (1.20 Å) and F (1.47 Å), minus an additional 0.2 Å) and four longer CH-F[S2] non-covalent interactions ($< \Sigma^{vdw}_{H\text{-}F} - 0.1$ Å) between ions, see Table S-1a for geometric details. Briefly, *anti*- slipped ($\beta = 12.4^o$) cofacial ($\alpha = 0^o$) stacking between pyridyl rings (perpendicular separation between mean planes 2.64 Å) of adjacent dications serves to assemble the centrosymmetric dications into polymeric chains along the *a*- axis (dashed cyan lines in Fig. S-3). The chains are further assembled in the remaining two directions by a concerted set of π-π and CH-π interactions involving three pyrazolyls (actually six per dication due to inversion symmetry). That is, the pyrazolyl containing N31 of one dication acts as a CH-π donor to the pyrazolyl containing N11 [C32H32 ··Ct[N11] 2.59 Å, 148^o) and is also involved in a tilted ($\alpha = 17.2^o$), slipped ($\beta = 15.1^o$; $\gamma = 31.3^o$) π-π interaction with the pyrazolyl containing N21 [Ct(N31)-Ct(N21) = 3.62 Å]; both of the latter pyrazolyl rings [Ct(N11) and Ct(N21)] are bound to the same methine carbon of a neighboring dication. This three dimensional structure is completely bolstered by (or could be reconstructed by only considering) the shortest five CH-F non-covalent interactions involving the acidic methine hydrogens (H1), meta-pyridiyl hydrogen H3, and pyrazolyl hydrogens H13, H21 and H23 and the four fluorides of the tetrafluoroborate anions, as detailed in Table S-1a.

The supramolecular structures of **2·CH$_3$CN** and **3·CH$_3$CN** are also three dimensional but are held together by less extensive networks of relatively weak non-covalent interactions compared with those in the structure of **1**. In fact, some of these interactions

in **2·CH$_3$CN** and **3·CH$_3$CN** are known to be quite weak as they involve the solvated molecules which were found to be easily removed upon drying under vacuum. Regardless, the structure of **2** is held together solely by weak hydrogen bonding interactions of the CH-F and one CH-N[S3] variety (this latter involving solvated CH_3CN); there are no CH-π or π-π interactions within acceptable metric ranges. For instance, although pyridyl rings of neighboring dications are coplanar and have perpendicular separations of 3.34 Å, the slip angle is large enough ($\beta = 46^o$) to force a very long centroid-centroid separation of 4.84 Å precluding any π-π stacking interactions. Instead, it is found that the two shortest CH-F interactions described in Table S-1b between acidic methine hydrogens and the tetrafluoroborate acceptors C1H1-F1 (2.38 Å, 157^o) and C7H7-F3 (2.27 Å, 160^o) combined with the inversion symmetry of the dication are sufficient to generate a corrugated sheets in the (10$\bar{1}$) plane as in Figure S-4a. The acetonitrile molecules of solvation are lodged within the sheet stricture via a longer CH-F interaction (purple dashed lines, Figure S-4a, C2sH2Sb-F1: 2.52 Å, 135^o) and two short CH-N interactions (green dotted lines, Figure S-4a) involving each end of CH_3CN and spanning neighboring dications. Specifically the methyl hydrogen H2Sa of acetonitrile acts as a donor to the pyridyl nitrogen N1 of one dication (C2sH2Sa-N1: 2.49 Å, 166^o) while the nitrile nitrogen N1s acts as an acceptor to the acidic pyrazolyl ring hydrogen H41 of an adjacent dication (C41H41-N1s: 2.51 Å, 166^o). The sheets are stacked in the third dimension via a pair of 'chelating' CH-F interactions (Figure S-4b) occurring between the *para*-pyridyl hydrogen donor H4 and F2 and F4 weak hydrogen bond acceptors of a single tetrafluoroborate anion with C4H4-F2 (2.53 Å, 131^o) and C4H4-F4 (2.54 Å, 158^o).

The supramolecular structure of **3·CH$_3$CN** is also three dimensional where multiple concerted CH-π interactions involving dimethylpyrazolyls groups organize the dications into sheets in the *bc*- plane while CH-F interactions involving the weakly-bound acetonitrile solvate (removed by drying under vacuum) serve to assemble the sheets in the third dimension, as illustrated in Figure S-5. More specifically, a set of four concerted CH-π interactions between adjacent dications involving three pyrazolyls, bound to one silver, in each metallacycle (Figure S-5b and Scheme S-1) act in concert to

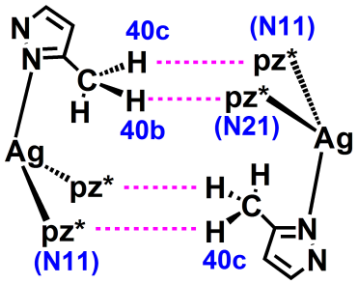

afford

Scheme S-1. Illustration of concerted CH-π interactions giving polymer along the b-axis.

a polymer that propagates along the *b*-axis. The pyrazolyl rings containing N11 and N21 act as acceptors to two of the three 3-methyl hydrogens from a the pyrazolyl ring containing N41 of an adjacent cation such that one interaction [C40H40c-Ct(N11) (2.69 Å, 146o)] is clearly shorter and presumably stronger than the other [C40H40b-Ct(N21) (2.98 Å, 156^o)]. The fourth pyrazolyl bound to silver acts as a donor in a set of CH-π interactions [Figure S-5c, C34H34c-Ct(N41) (2.80 Å, 139^o)] that assemble the chains into sheets. The tetrafluoroborate anions are anchored to each dication via three short CH-F interactions involving a methine and two 5-methylpyrazolyl hydrogens. Specifically, as

shown in Figure S-5a, F2 is involved in a bifurcated set of CH-F interactions with the methylpyrazolyl hydrogens H34a (C34H34a-F2; 2.39 Å, 137^{o}) and H24b (C24H24b-F2; 2.47 Å, 167^{o}). An additional CH-F interaction between F1 and a methine hydrogen (C7H7-F1; 2.47 Å, 133^{o}) locks the tetrafluoroborate on the *exo*- side of the pyridyl ring with F3 oriented toward the neighboring dication. The acetonitrile molecules of salvation link the dications into chains along the *a*- axis by a set of rather short CH-N and CH-F interactions involving each end of the molecule. The acidic hydrogen of acetonitrile methyl acts as a donor in a CH-F interaction with the aforementioned F3 (C2SH2Sc-F3; 2.38 Å, 124^{o}) of the tetraflouroborate associated with one dication while the nitrile nitrogen acts as an acceptor in a weak CH-N interaction (C14H14b-N1S; 2.55 Å, 139^{o}) involving the 5-methyl pyrazolyl hydrogen of a neighboring dication.

Finally, although the poor quality of the structure of **5** precludes meaningful analysis of its supramolecular structure, it can be seen in Figure S-6, that there are no unusually close contacts between cation chains. That is, the isopropyl substituents protect the heterocyclic groups from entering into extensive non-covalent interactions limiting the closest contacts between CH···O functionalities of the cation and anion respectively.

Figure S-7. X-Ray Powder diffraction pattern of (a) vacuum dried sample as-formed powder of **2** (top, maroon) versus the calculated diffraction pattern of **2**·CH_3CN (blue, bottom) based on single crystal diffraction experiment; (b) as-formed powder of **4**; and (c) vacuum dried as-formed powder of **5** compared to diffraction pattern calculated from single-crystal diffraction data.

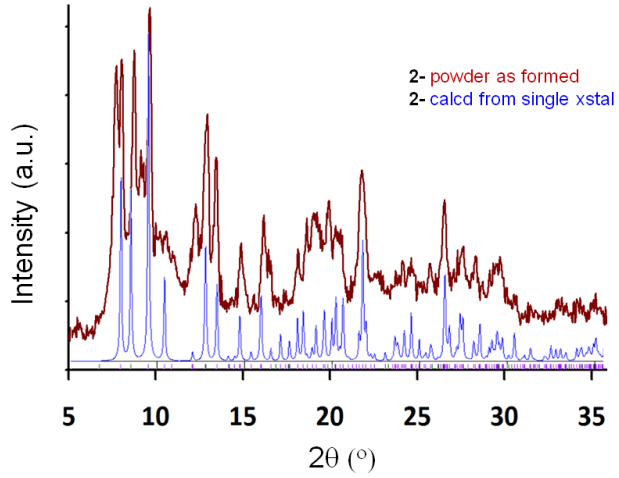

(a)

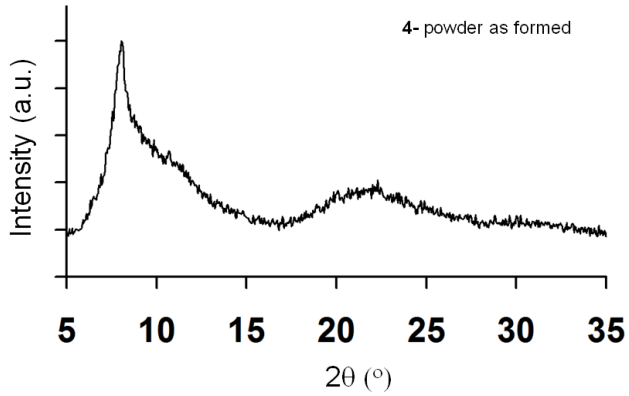

(b)

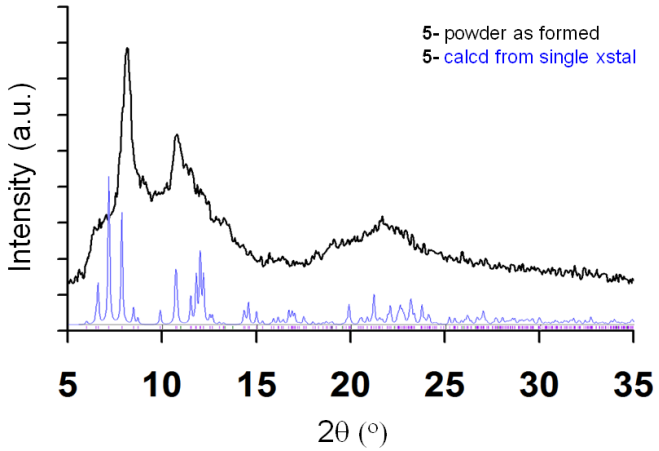

(c)

Details of the PFGSE ^{1}H NMR Experiments. PFGSE experiments were preformed on a Varian Unity-Inova 400 insturment with z-axis gradient coil. The gradient field *G* from 0 to 60 G/cm was calibrated using the diffusion coefficient of H_2O in D_2O.[S4] Diffusion measurements were made on non-spinning samples in CD_3CN maintained at 295 K. The gradient field *G* was varied between 1 and 60 G/cm in ten steps. The standard Varian DBPPSTE spin echo sequence was employed which used 2 ms pulses and 100 ms delay between pulses to develop echoes. Diffusion coefficients were determined using Varian PGE software and by manual calculations of signal intensity versus gradient field. For the latter, the relation $\ln(I/I_o) = -\gamma\delta^2G^2(\Delta-\delta/3)D$ was used where δ is the length of the gradient pulse (0.002 s), Δ is the delay between pulses (0.1 s), γ is the proton magnetogyric ratio, and D is the diffusion coefficient. These calculations were performed on at least two or three resonances (the methine, the 4-pyrazolyl, *p*-pyridyl or a methyl) if possible, for each spectrum of a given compound and the mean values for the diffusion coefficients were used to obtain the hydrodynamic radii. For the measurements of ligand diffusion, solution mixtures approximately 0.05 M in the desired ligand, and in $Ga(acac)_3$ as an internal reference or including 0.05 M of additional ligand gave consistent results. For measurement of silver(I) complexes, $[Ru(bpy)_2(CH_3CN)_2](BF_4)_2$ was added as a reference. The references were chosen owing to the similarities with compounds and complexes being examined in terms of their known size,[S5][S6] their comparable (molecular versus ionic) nature, their mutual inertness with respect to reactions with the compounds, their distinctive chemical shifts, due to their ready availability in our laboratory, and for the former, its previous successful employment in a similar study.[S7] The hydrodynamic radii were calculated by applying the Stokes-

Einstein relation, $R_H = kT/(6\pi\eta D)$ where R_H is the hydrodynamic radius, η is the viscosity of the solution which is assumed to be close to that of the pure solvent (0.384 mPa·s or cP) at 295 K,[S8][S9][S10] and then confirmed from the constant R_H values obtained from the reference compounds and the ligands over the concentration ranges used. Attempts were made to perform the experiments at either high or low temperature but these did not give reliable (consistent) data owing to problems with the known large changes in viscosity with temperature for acetonitrile (especially convection at high temperature), solubility issues, and possibly differing degrees of association at low temperatures.

Table S-2. PFGSE NMR data for the $pz^{R}{}_{4}lut$ ligands, their silver(I) complexes **1**-**5** and reference compounds $Ga(acac)_3$ and $[Ru(bpy)_2(CH_3CN)_2](BF_4)_2$] used to generate Figures 8 in main text.

	ln (I/Io)				
$G^2(G/cm)^2$	**pz_4lut**	**$pz^{4'}{}_4lut$**	**$pz^{*}{}_4lut$**	**$pz^{DIP}{}_4lut$**	$Ga(acac)_3$
4.3681	0	0	0	0	0
17.4724	-0.08097	-0.02667	-0.07042	-0.0493	-0.02828
39.3129	-0.10536	-0.09663	-0.10093	-0.08724	-0.08304
69.8896	-0.23713	-0.2036	-0.21319	-0.19199	-0.23971
109.2025	-0.34093	-0.3234	-0.32296	-0.29191	-0.38965
157.2516	-0.49248	-0.41871	-0.43386	-0.39164	-0.53162
214.0369	-0.62861	-0.64185	-0.59421	-0.53647	-0.70517
279.5584	-0.86222	-0.80437	-0.78526	-0.70589	-0.97158
353.8161	-1.06582	-1.07264	-0.96758	-0.89129	-1.24187
436.81	-1.32176	-1.28621	-1.19073	-1.08854	-1.4824

	ln (I/Io)				
$G^2 (G/cm)^2$	**1**	**2**	**3**	**5**	$[Ru(bpy)_2(CH_3CN)_2]^{2+}$
4.3681	0	0	0	0	0
17.4724	-0.10536	-0.07925	-0.05314	-0.02844	-0.11292
39.3129	-0.17067	-0.1423	-0.11394	-0.07435	-0.13853
69.8896	-0.27625	-0.24883	-0.2214	-0.14742	-0.26669
109.2025	-0.38668	-0.3574	-0.32812	-0.22626	-0.45169
157.2516	-0.58228	-0.5339	-0.48551	-0.3598	-0.59728
214.0369	-0.76461	-0.71169	-0.65878	-0.50875	-0.77662
279.5584	-0.99705	-0.94801	-0.89896	-0.6655	-1.07628
353.8161	-1.31317	-1.23914	-1.16511	-0.8298	-1.32073
436.81	-1.57554	-1.50016	-1.42479	-0.97565	-1.56329

Figure S-8. Downfield region of the ^{1}H NMR spectra of **1** in CD_3CN at 20 K increments between 293K and 233 K.

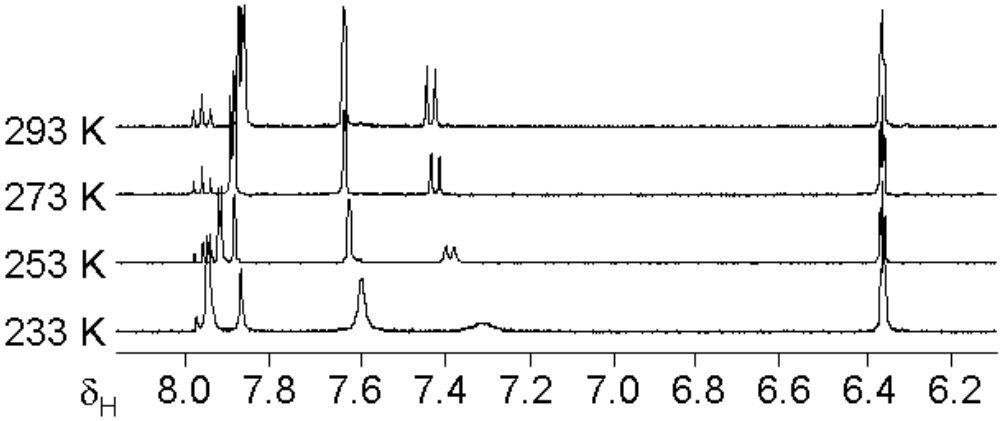

Figure S-9. Portions of the variable temperature ^{1}H NMR spectra of **2** in CD_3CN in 5 K increments between 293K and 233 K.

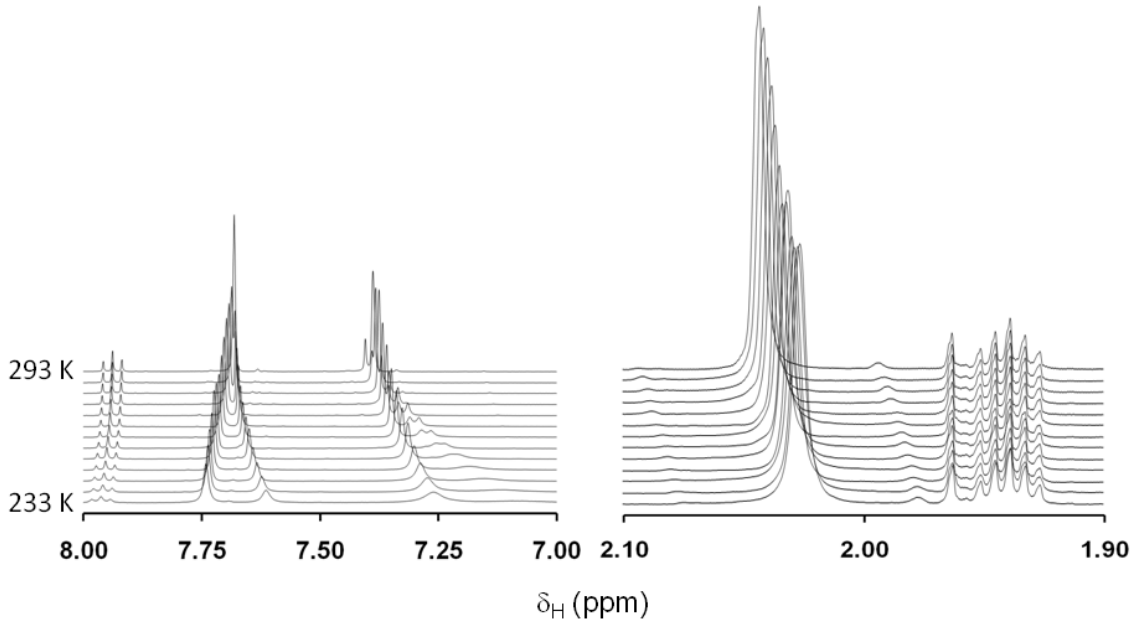

Figure S-10. Variable Temperature ^{1}H NMR spectra of **3** in CD_3CN.

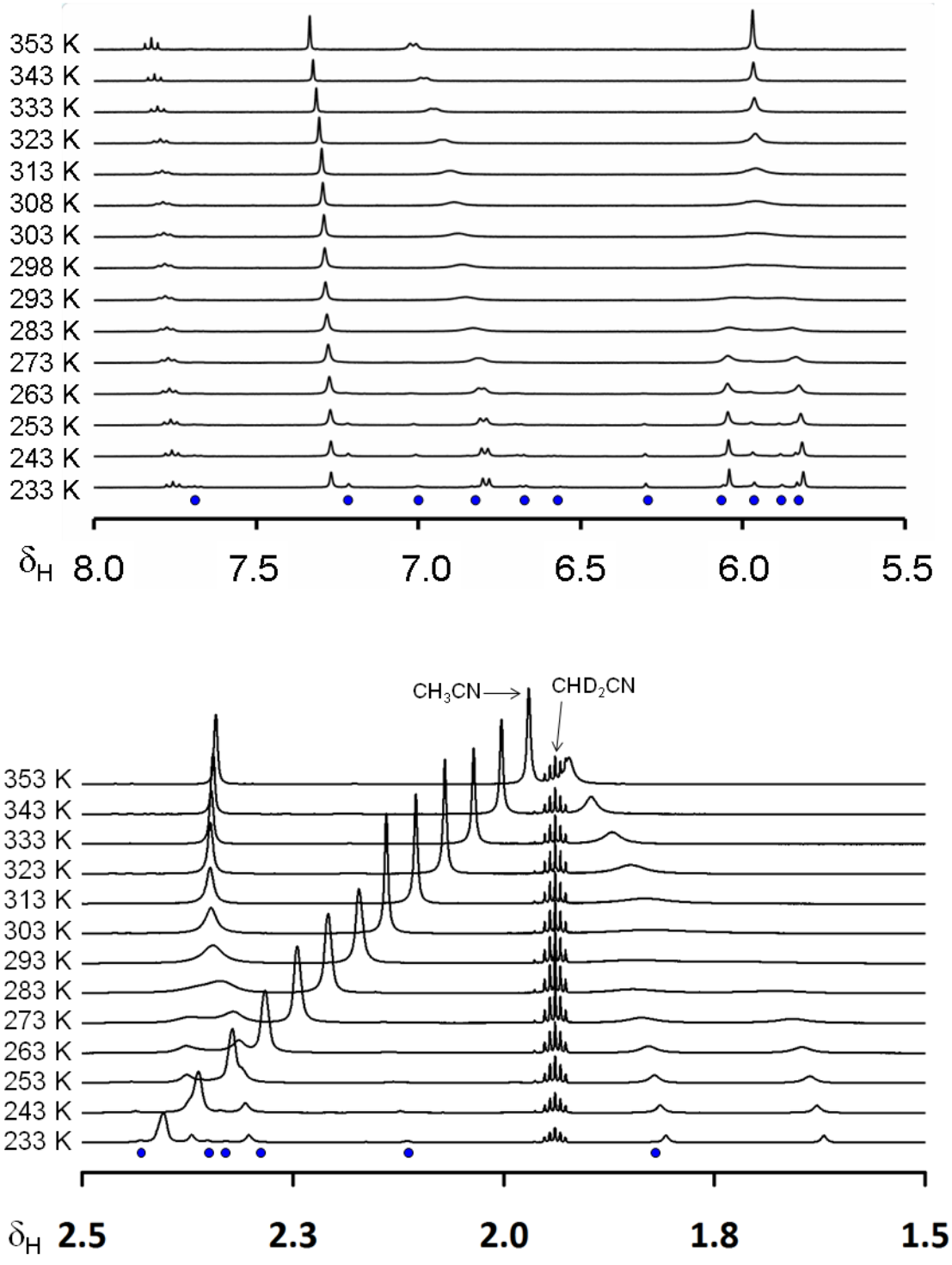

Figure S-11. (a) Downfield and (b) Upfield Portions of the ^{1}H NMR spectra of **4** in CD_3CN acquired at 20 K intervals from 233K (bottom spectrum) to 353 K (top spectrum). Solvent impurity resonances occur at 7.6 and between 2.5 to 1.9 ppm

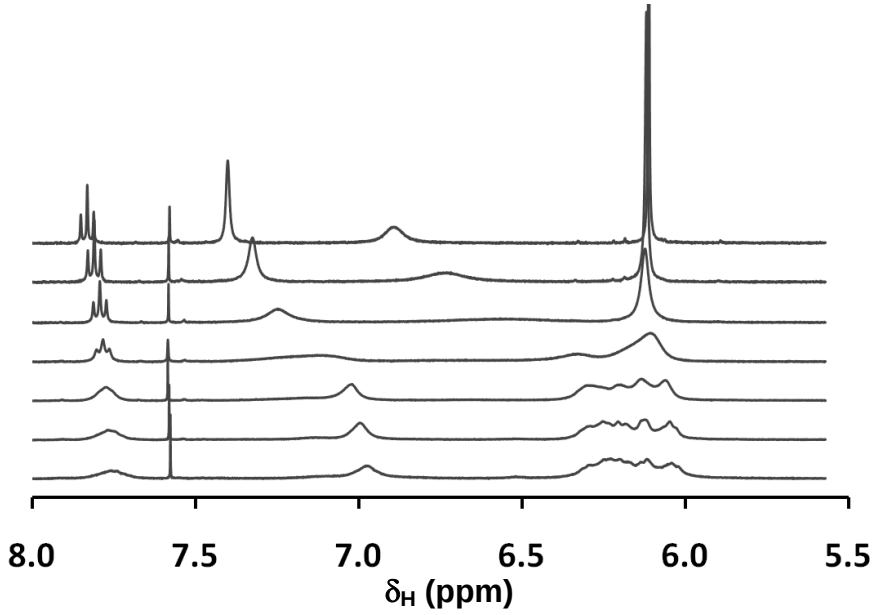

(a)

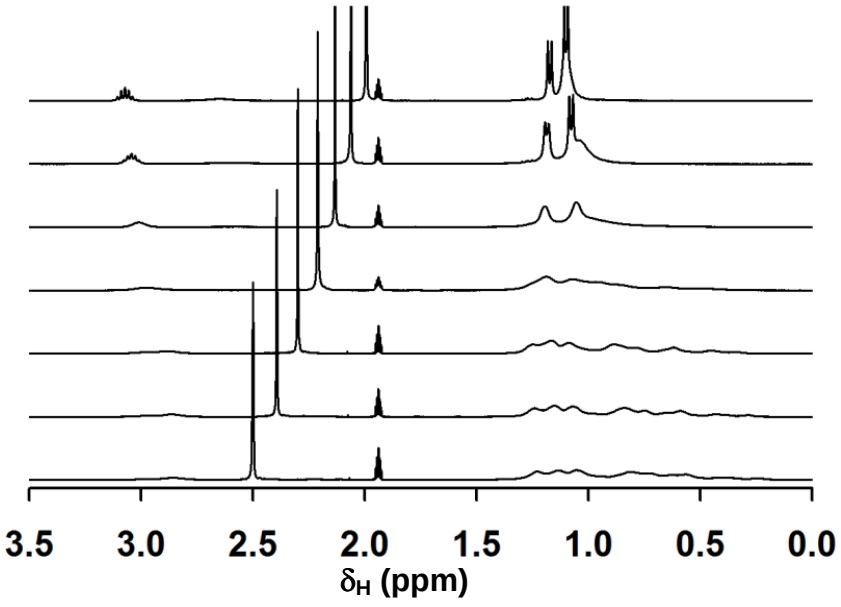

(b)

Figure S-12. Variable Temperature ^{1}H NMR spectra of **5** in CD_3CN. Note that in this case, the high (> 293 K) and low temperature (≤ 293 K) spectra were recorded for two different samples, as indicated by the different solvent impurity resonances occurring between 2.5 to 2.0 ppm. This observation illustrates the negligible effect of changes in concentration of **5** on the resonances for the cation.

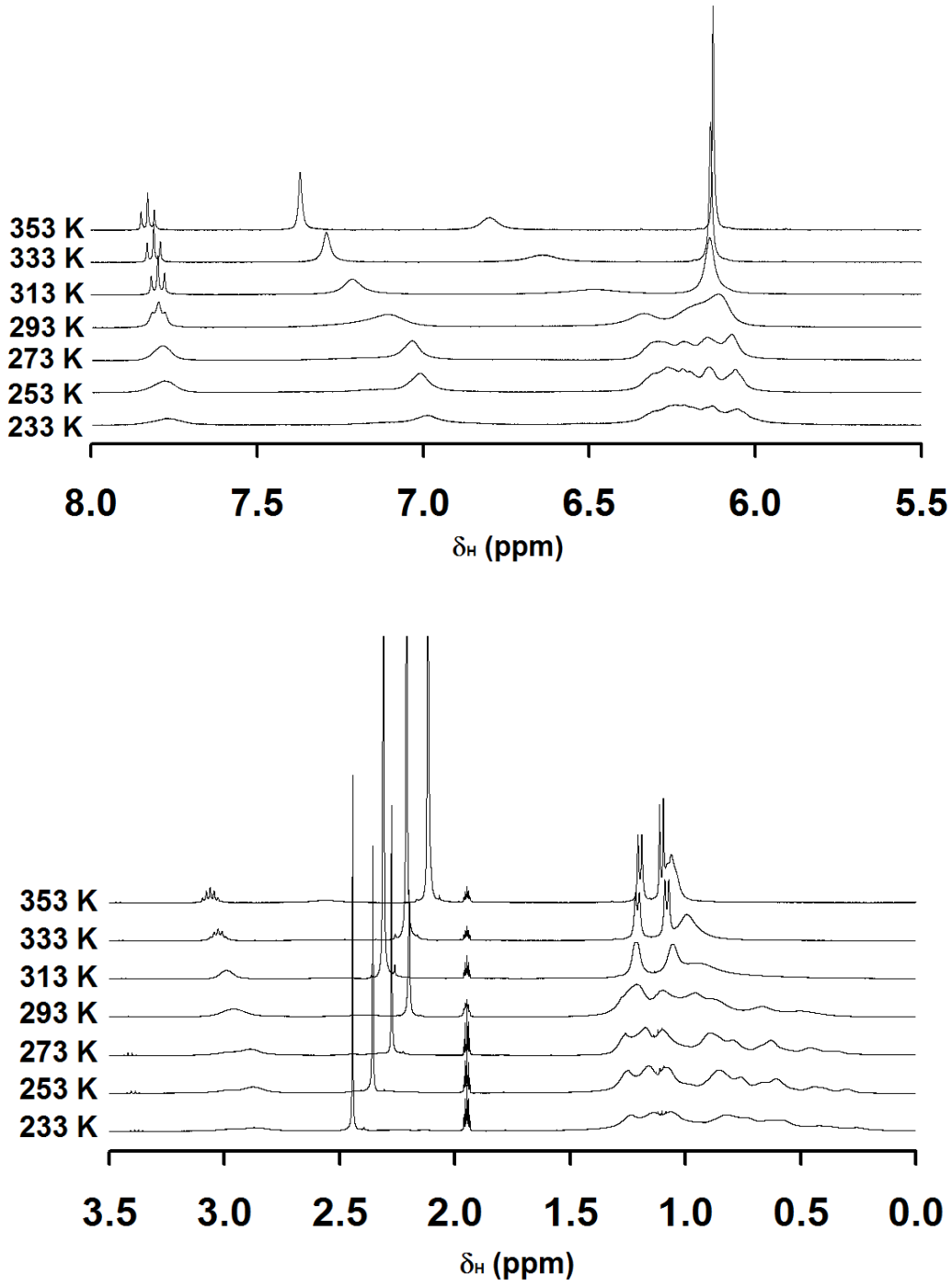

Discussion of the Variable Temperature ^{1}H NMR spectra. The spectra of each **1**-**5** were acquired from 233 K to 353 K (over the liquid range of CD_3CN) and results are shown in Figures S-8 to S-12. A comparison of the Figures reveals the temperature dependence of the spectra for **1** and **2** is slightly different than that for **3**-**5**, thus the former two will be discussed separately from the latter three. For complexes **1** and **2**, the number of resonances of remains constant but the resonances for the *meta*- hydrogens of the pyridyl group (doublet centered near 7.4-7.2 ppm) experience the greatest change in both chemical shift and in line-broadening with temperature. The resonances for the methine and the 5- hydrogens of the pyrazolyl groups (near 7.9 ppm for **1** and in the 7.8-7.6 range for **2**) change to a lesser degree than those for the *meta*- pyridyl hydrogens but more so than the remaining resonances which are only little affected by changes in temperature. Although coalescence was not reached, line shape analyses[S12] based on the broadening of 5-pyrazolyl hydrogen resonances gave energy barriers for exchange of 10.8 ± 0.1 kcal/mol for **1** and 11.3 ± 0.1 kcal/mol for **2**. Spectral changes similar to those found for **1** and **2** are observed for complexes **3**-**5** but the slow exchange limit is attained. The latter three complexes were found to possess identical activation barriers of 14.3 ± 0.1 kcal/mol for **3** and 14.4 ± 0.1 kcal/mol for **4** and **5** based on both line shape analyses as above and by using the standard relation $E_a = 4.57T_c[10.32+\log(\sqrt{2}T_c/\pi\Delta\nu)]$ (where T_c is the coalescence temperature of various selected resonances and $\Delta\nu$ is the chemical shift difference of the resonances in absence of exchange).[S13] The spectrum for **3**-**5** are further complicated by the formation of new, possibly multiple, species at low temperature. The large number of overlapping, multiplet resonances of weak intensity for **3**, and the broad nature of the signals for **4** and **5**, all conspire against successful

unambiguous assignment. Of the three complexes, the variable temperature spectra for **3** are the most revealing. That is, as exemplified by the downfield region of the spectra for **3** shown in Figure S-10 (page S-17). At high temperature only one set of resonances are observed for each type of ligand hydrogen. Upon cooling the solution of **3**, the three single resonances for each type of pyrazolyl group hydrogen (4-H and including the 3-methyl and 5-methyl not shown) broaden and decoalesce near room temperature to give six total resonances (two of each type) that sharpen as exchange is slowed by further lowering temperature. Concomitantly, the pyridyl hydrogen resonances shift upfield, lose and regain coupling features, but do not split into multiple resonances on cooling. However, new sets of ligand resonances appear from the baseline at about 263 K and grow in intensity when the temperature is lowered to 233 K (Figure S-13), behavior

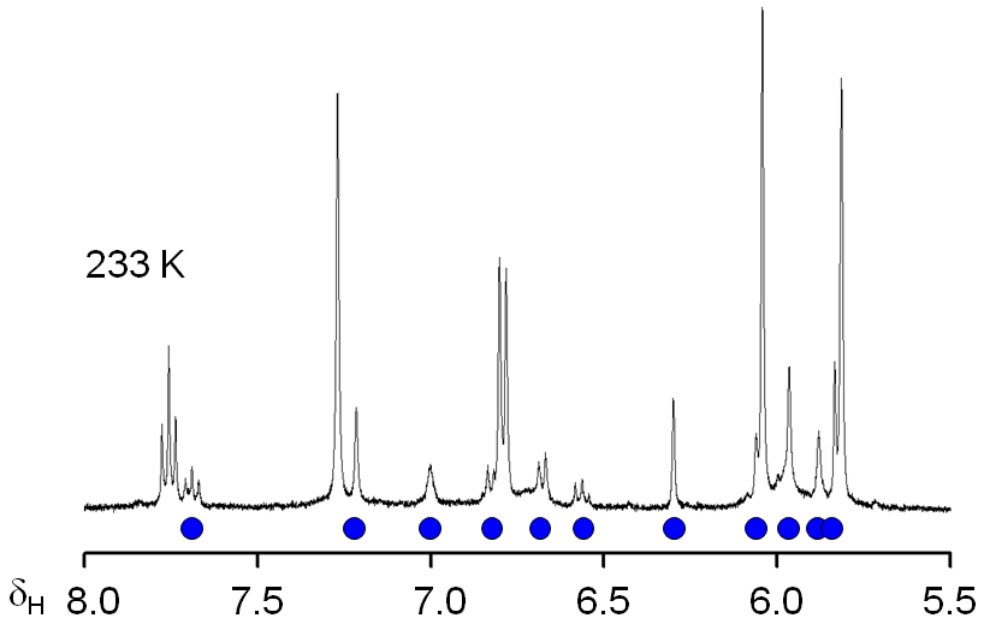

Figure S-13. The downfield region of the ^{1}H NMR spectrum of **3** in CD_3CN acquired at 233 K emphasizing resonances for new unidentified species at appearing at low temperature (blue circles).

indicative of the equilibrium formation of multiple species at low temperature. Again, similar behavior is observed for the (low temperature) spectra of **4** and **5** (Figures S-11 and S-12) but the latter are but more complicated owing to the larger number of broader multiplet resonances which may be further exacerbated by the different extent of oligomerization.

Disregarding the stereochemistry at the methine carbon atoms, there are thirteen distinct coordination modes for the ligand in monomeric $[AgL]^+$ complexes that are capable of giving species that span only four different point groups (C_{2v}, C_2, C_s, and C_1) as illustrated in Figure S-14. Thus, even before considering any dynamic behavior typical of silver(I) (and even with a known crystal structure), assigning solution structures based solely on the number and types of resonances appearing in the NMR spectrum is intrinsically problematic and, for all practical purposes, is likely an

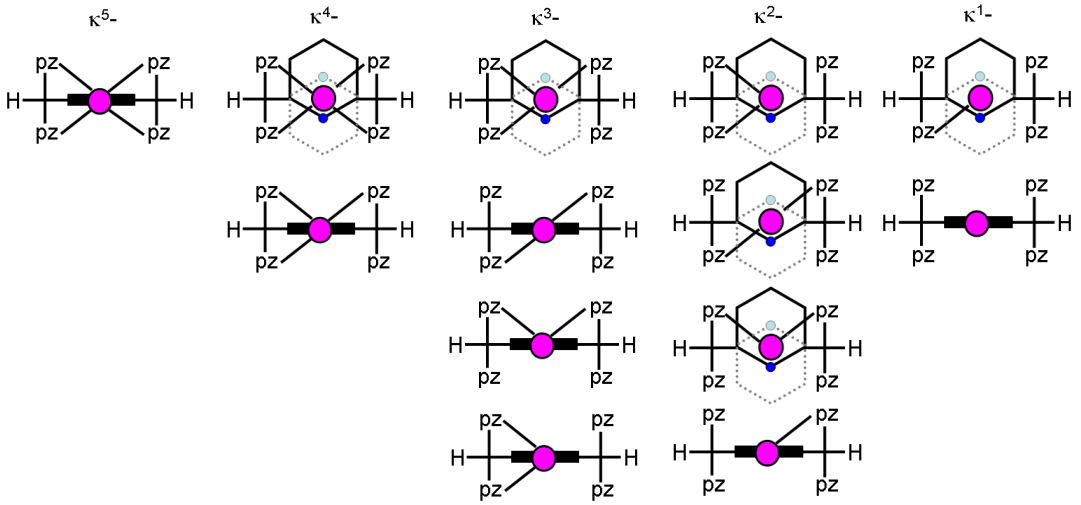

Figure S-14. Cartoon depictions of coordination modes of ligands in monomeric $[AgL]^+$ complexes. The denticity of ligand decreases from left (κ^5-) to right (κ^1-). Larger (magenta) spheres represent $[Ag(CH_3CN)_{0\text{-}3}]^+$; blue spheres represent unbound pyridyl nitrogen; thick black bar represents planar silver-bound pyridyl; dotted hexagon is an alternate conformer of unbound pyridyl with solid outline.

intractable problem based on the data at hand. Nonetheless, after contemplating the cumulative solution NMR behavior and mass spectral data of **1**-**5** and of related silver complexes, we tentatively favor a scenario where at high temperature, rapid interchange between κ^1- and κ^2- bound ligands (right half of Figure S-14) affords exchange-averaged pyrazolyl group resonances in the dynamic solution process. In this situation, alkyl-substitution on the pyrazolyls contributes to increasing the activation barrier by inductive electronic effects (via strengthening the Ag-N bond) and by restricting C-C and C-N bond rotations involving pyrazolyls and the pyridyl groups around methine carbons via steric interactions (we are neglecting any added effects from silver-bound solvent molecules). At modestly low temperature, the C_s symmetric κ^2- structure (second from the bottom of Figure S-14) would necessarily predominate giving two sets of pyrazolyl signals. A κ^1-ligand also simplifies explanations regarding the facile free/bound ligand exchange processes. That is, the addition of excess free ligand to the solutions of **1**-**5** gives only exchange-averaged signals rather than discrete resonances for each the free ligand and the corresponding silver complex, a process that would be far more easily rationalized for a monomeric species versus a dimeric dication. At very low temperature the newly observed peaks in **3**-**5** could be accounted for by the formation of either cyclic or linear oligomers (as in the top of Figure S-15) or, less satisfactorily from a self-assembly point of view, by the preferential formation of any of the C_1-symmetric (κ^3, κ^2, or κ^1) monomeric cations. Again, the alternative possibilities such as rapid interchange between k^2-/k^3-, k^3-/k^4-, or κ^4-/κ^5- bound silver (left half of Figure S-14) cannot be excluded. The latter is disfavored considering the preference of silver(I) for low coordination numbers (typically ≤ 4), the relatively high activation energy anticipated for

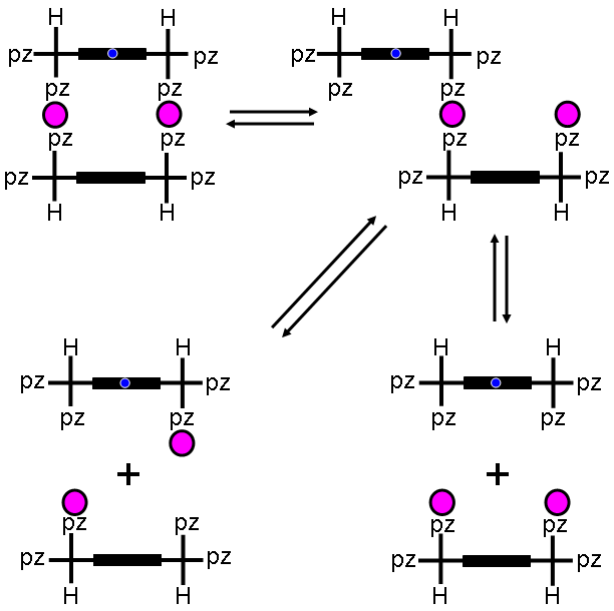

Figure S-15. Proposed equilibria controlling self-assembly and ligand exchange.

Ag-N(pyridyl) bond dissociation and rotation while maintaining Ag-N(pz) bonds (compared to the low energy of the observed activation barriers of 10-14 kcal/mol). Moreover, these alternatives do not easily account for the facile ligand exchange or the disparity in self-assembly with changes in pyrazolyl substitution (Figure S-15). It should be re-emphasized that even if a crystal structure of a monomeric species were known, assignment of the solution structure based on the number of resonances would still remain tenuous.

Figure S-13. ESI(+) mass spectrum of **1.**

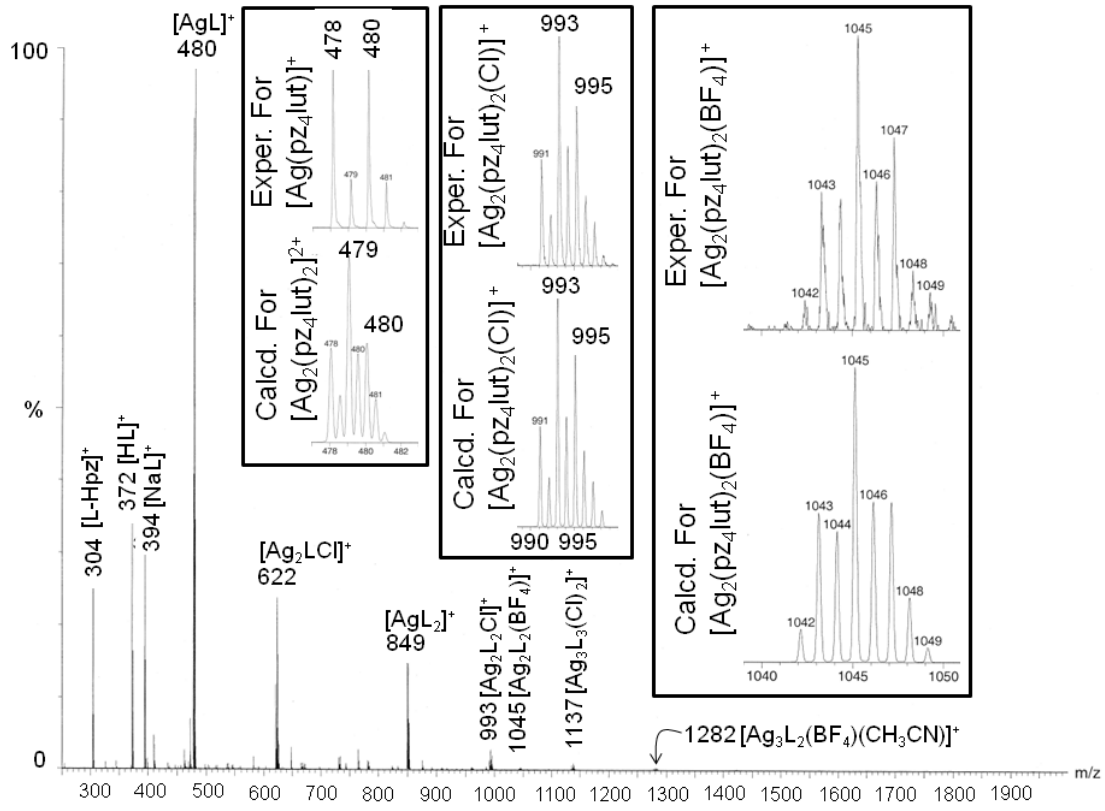

Figure S-14. ESI(+) mass spectrum of **3.**

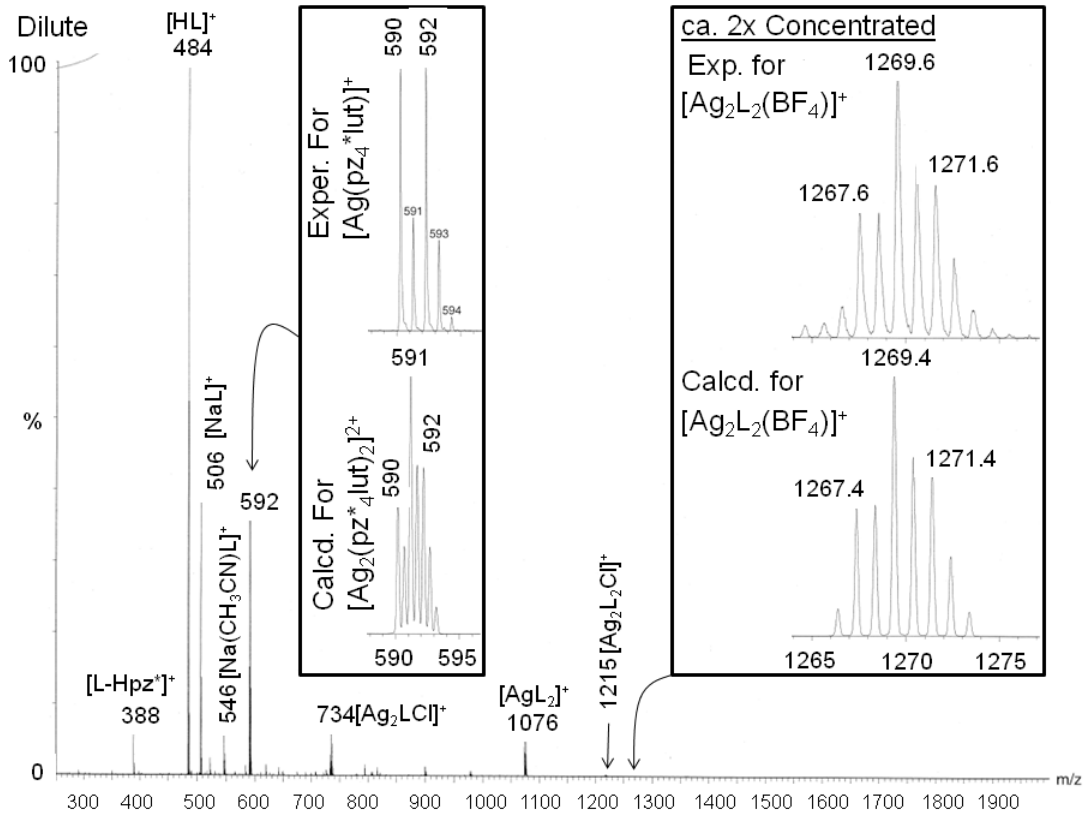

Figure S-15. ESI(+) mass spectrum of **4.**

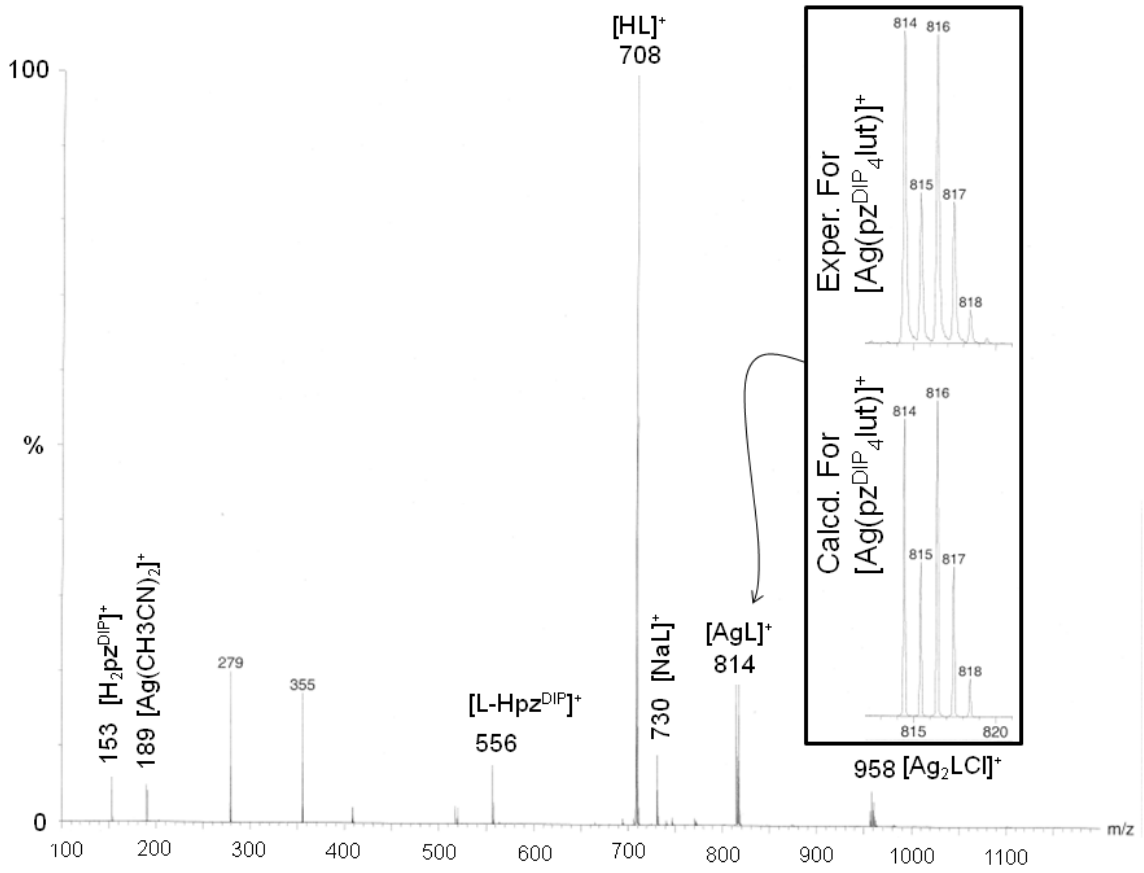

Figure S-16. ESI(+) mass spectrum of **5.**

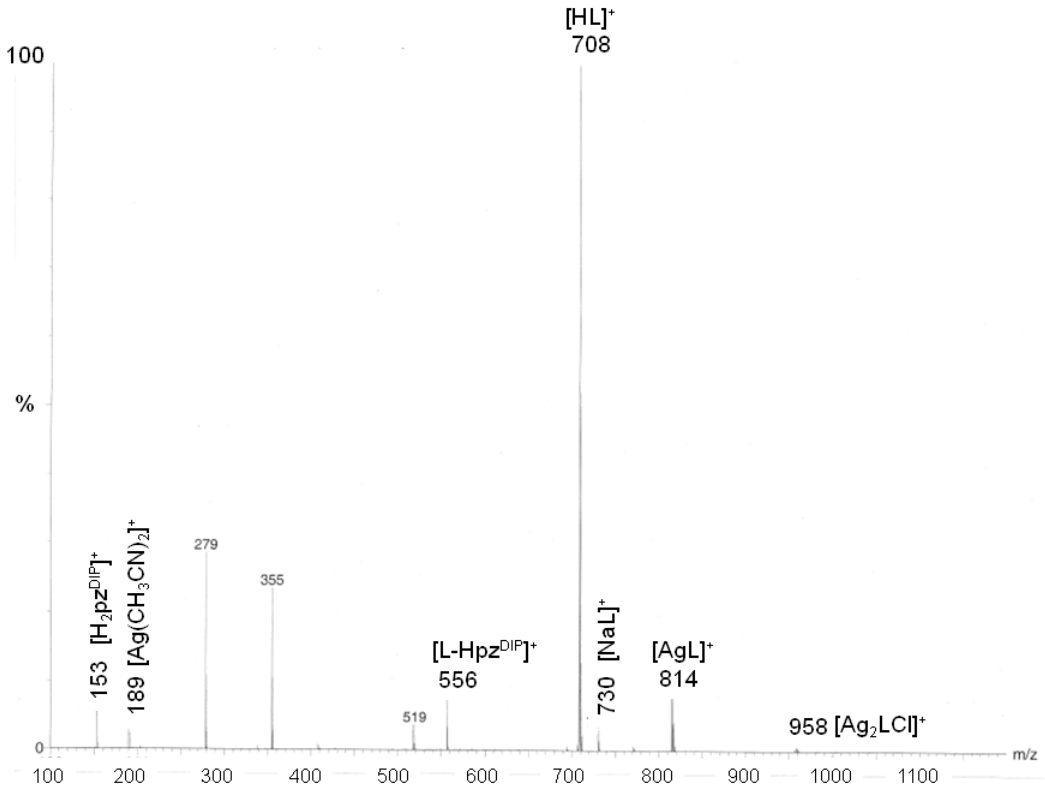

References

[S1] (a) Janiak, C. *J. Chem. Soc., Dalton Trans.* **2000**, 3885.

(b) Reger, D.L.; Gardinier, J.R.; Semeniuc, R.F; Smith M.D. *Dalton Trans.* **2003**, 42, 7635. (c) Reger, D.L., Semeniuc, R.F.; Smith, M.D. *Cryst. Growth Design* **2005**, *5*, 1181.

[S2] Grepioni, F.; Cojazzi, G.; Draper, S.M.; Scully, N.; Braga, D. *Organometallics*, **1998**, *17*, 296.

[S3] Taylor, R.; Kennard, O. *J. Am. Chem. Soc.* **1982**, *104*, 5063.

[S4] Masuda, A.; Ushida, K.; Koshino, H.; Yamashita, K.; Kluge, T. *RIKEN Review*, **2002**, *45*, 31.

[S5] Dymock, K.; Palenik, G.J. *Acta Cryst. B* **1974**, *30*, 1364. Hydrogens were placed in idealized positions and the diameter was measured using the average of the three most distal H···H separations.

[S6] Heeg, M.J; Kroener, R.; Deutsch, E. *Acta Cryst. Sect. C*, **1985**, *41*, 684.

[S7] Reger, D.L.; Gardinier, J.R.; Pellechia, P.J.; Smith, M.D.; Brown, K.J. *Inorg. Chem.* **2003**, *42*, 7635.

[S8] D.R. Lide, Ed.; *CRC Handbook of Chemistry & Physics*, 74th Ed., CRC Press: Boca Raton, USA (1993).

[S9] Gilmont, R. *Chem. Eng. Prog. Mag.* **2002**, *98(10)*. 36.

[S10] Given the values for viscosity of acetonitrile reported in CRC Handbook at 25 ^{o}C, 50 ^{o}C, and 75^{o}C (0.369, 0.284, 0.234 cP, respectively) and elsewhere see ref [S11], it was found necessary to use corrected values for parameters in reference [S9] of log η_o (= log μ_o in reference = log of viscosity at 21.1^{o}C) = -0.4161 and G

= 314.9 to obtain a reasonable value of viscosity (0.384 cP) at 22^{o}C, the temperature of the experiment. These corrected parameters were obtained using the CRC values at high temperature (> 0^{o}C) and applying methodology in reference [S9]. That is, a plot of log η versus Z [= 1/(T(^{o}C)+233) – 1/(21.1+233)] gave a least squares best fit line of log η = GZ + log η_o = 314.9*Z -0.4161 with R^2 = 0.9988. The large change in viscosity of CH_3CN at low temperature provides a very poor fit for the CRC value η = 0.400 cP at 0^{o}C.[S8]

[S11] (a) K. Ibuki and M. Nakahara. *J. Phys. Chem.*, **1990**, 94, 8370. (b) K. Das, K.D. Ashby, J. Wen, and J.W. Petrich. *J. Phys. Chem. B,* **1999**, 103, 1581. (c) Kennedy, K.G.; Miles, D.T. *J. Undergrad. Chem. Res.* **2004**, *4*, 145.

[S12] (a) Reich, H. J. . WinDNMR: Dynamic NMR Spectra for Windows *J. Chem. Educ. Software* **3D2** (created 1996) (b) Reich, H.J.; Goldenberg, W.S.; Gudmundsson, B.Ö.; Sanders, A.W.; Kulicke, K.J.; Simon, K.; Guzei, I.A. *J. Am. Chem. Soc.* **2001**, *123*, 8067-8079.

[S13] Kessler, H. *Angew. Chem. Int. Ed.***1970**, *9*, 219.